PCCP

ROYAL SOCIETY OF CHEMISTRY

PAPER

Cite this: *Phys. Chem. Chem. Phys.*, 2026, **28**, 4862

Exploring the cyclization reaction channel for the gas-phase elementary reaction between the silicon nitride radical (SiN, $X^2\Sigma^+$) and isoprene (C_5H_8, X^1A') to prepare methylazasilacyclo-hexadienylidenes ($SiNC_5H_7$, X^1A')

Surajit Metya, [a] Iakov A. Medvedkov, [a] Daniel González, [a] Shane J. Goettl, [a] André K. Eckhardt *[b] and Ralf I. Kaiser *[a]

Received 9th November 2025,
Accepted 26th January 2026

DOI: 10.1039/d5cp04314j

rsc.li/pccp

Silicon-containing heterocyclic molecules have emerged as promising candidates in medicinal and agrochemical research. However, the synthesis of silicon-containing heterocycles has remained highly challenging. In this work, we employed the crossed molecular beams technique to elucidate the underlying reaction pathways for the synthesis of a unique class of six-membered cyclic organosilicon molecules in which silicon and nitrogen atoms occupy adjacent positions: methyl-azasilacyclohexadienylidenes – silicon and nitrogen substituted benzenes functionalized with a methyl group. This class was accessed *via* the reaction of ground-state silicon nitride radicals (SiN, $X^2\Sigma^+$) with isoprene (C_5H_8, X^1A') under single-collision conditions at a collision energy of 25 ± 1 kJ mol^{-1}. Integration of experimental results with electronic structure calculations revealed the formation of at least two cyclic products: 4-methyl-1-aza-2-silacyclohexa-3,5-dien-2-ylidene and 5-methyl-1-aza-2-silacyclohexa-3,5-dien-2-ylidene. The underlying mechanism shows strong similarities to the previously studied reaction of the silicon nitride radicals (SiN, $X^2\Sigma^+$) with 1,3-butadiene (C_4H_6, X^1A_g), with the methyl group in isoprene classified as a spectator, thus advancing our fundamental understanding of the organosilicon chemistry through the delivery of synthetic pathways to a distinct class of silicon-containing heterocyclic molecules: methylazasilacyclo-hexadienylidenes.

Introduction

It is a well-established observation that nature exhibits a marked preference for heterocyclic molecules as integral segments or as molecular skeletons in the architecture of contemporary biomolecules.[1–3] Five- and six-membered heterocyclic molecules, whether saturated or unsaturated, containing one or more heteroatoms (Scheme 1), are of particular interest due to their fundamental role in the chemistry of life. In this context, the study of cyclization reactions holds a central place in chemical research, serving as a vital tool to probe the properties and reactivity of biomolecules. Generally, cyclization reactions proceed through a variety of intermediates, such as cationic, anionic, radical, or metal-complex species, each offering unique mechanistic insights and synthetic potential.[1] Over the past few decades, radical-mediated cyclization reactions have gained significant attention compared to other types of cyclization reactions for their synthetic utility, offering high regio- and stereochemistry under mild conditions with broad functional group

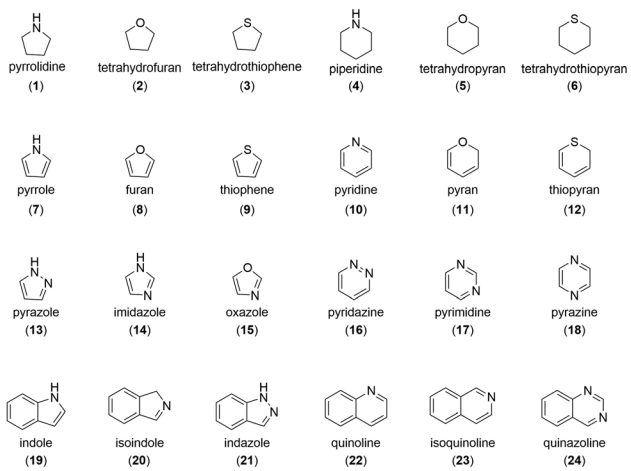

Scheme 1 Common heterocyclic moieties present in biomolecules.

[a] *Department of Chemistry, University of Hawai'i at Manoa, Honolulu, HI 96822, USA. E-mail: ralfk@hawaii.edu*
[b] *Organische Chemie II, Ruhr-Universität Bochum, Universitätsstraße 150, Bochum 44801, Germany. E-mail: andre.eckhardt@ruhr-uni-bochum.de*

tolerance.[4] Beyond preparative synthesis, these reactions are also of great interest in the field of gas-phase reaction dynamics, as they provide valuable insights into processes relevant to atmospheric chemistry and extraterrestrial environments.[5–10]

Contextually, radical-mediated cyclization reactions for synthesizing exotic heterocyclic molecules, particularly those containing silicon (Si), have attracted significant attention in recent years.[11–25] A major reason for this interest is the isovalency of silicon with carbon.[26] However, silicon differs markedly from carbon in several properties: silicon has a larger atomic radius (1.10 Å *vs.* 0.70 Å), lower electronegativity of 1.90 *versus* 2.55 on the Pauling scale, the ability to adopt higher coordination numbers *via* 3d orbitals, and a general inability to form stable double or triple bonds.[27–31] Interestingly, these differences often make silicon-substituted organic molecules environmentally friendly and non-toxic alternatives to their carbon analogues.[21,32–35] Despite this potential, the synthesis of silicon-containing heterocycles has remained challenging, and studies on their reaction dynamics are sparse. Yang *et al.* investigated the gas-phase synthesis of the five-membered silicon-containing heterocycle 1-silacyclopenta-2,3-diene (SiC_4H_6, X^1A_1) through the reaction of the silylidyne radical (SiH, $X^2\Pi$) with 1,3-butadiene (C_4H_6, X^1A_g) proceeding *via* doublet radical intermediates.[11] In our recent work, we synthesized an adjacent silicon–nitrogen-containing benzene-type heterocycle representing a special class of organosilicon molecules, through the gas-phase cyclization reaction using a crossed molecular beam machine. That study explored the reaction dynamics of silicon nitride (SiN, $X^2\Sigma^+$) and 1,3-butadiene (C_4H_6, X^1A_g), which yields two isomers of azasilabenzene: 1-aza-2-silacyclohexa-3,5-dien-2-ylidene and 1-aza-2-silabenzene (Fig. 1).[36] In contrast, the isovalent cyano radical (CN, $X^2\Sigma^+$) reacting with 1,3-butadiene (C_4H_6, X^1A_g) produces predominantly the acyclic product 1-cyano-1,3-butadiene rather than a pyridine-like ring.[37,38] These observations underscore that reaction dynamics for silicon variants can differ significantly from their carbon analogues. Several experimental and theoretical studies shows that the cyano radical (CN) reacting with hydrocarbons (C_xH_y) such as acetylene (C_2H_2),[39] ethylene (C_2H_4),[40] allene (H_2CCCH_2),[41] methylacetylene (CH_3CCH),[41] propene ($CH_2CH(CH_3)$),[41] and benzene (C_6H_6)[42] predominantly produces organic nitriles (RCN) *via* unimolecular decomposition involving hydrogen loss, with no evidence of isonitrile (RNC) formation. By contrast, analogous reactions with isoelectronic silicon nitride radical (SiN) predominantly yield silaisonitriles (RNSi), as the unpaired electron of the radical resides on the nitrogen atom due to the lower electronegativity of silicon.[43,44]

In this work, we present the reaction dynamics of the cyclization channel in the reaction between silicon nitride (SiN, $X^2\Sigma^+$) and isoprene (2-methyl-1,3-butadiene; C_5H_8, X^1A'), leading to the formation of six-membered heterocyclic molecules containing adjacent silicon and nitrogen: 4-methyl-1-aza-2-silacyclohexa-3,5-dien-2-ylidene and 5-methyl-1-aza-2-silacyclohexa-3,5-dien-2-ylidene. This study is conducted under single-collision conditions, exploiting a crossed molecular beam apparatus combined with electronic structure and statistical calculations.[41,45–49] The reaction dynamics of gas-phase cyclization reactions between two acyclic reactants proceeded *via* radical intermediates and can be explored using the crossed molecular beam technique, which provides a clean and controlled synthesis environment.[11] A key advantage of the crossed molecular beam technique over traditional preparative methods is that both reactants can be independently generated in separate source chambers in distinct molecular beams. The reaction products then exit the collision zone without any interference, allowing for clean detection *via* a differentially pumped quadrupole mass spectrometer.[6,47,50,51] Therefore, this molecular-level investigation, supported by electronic structure calculations, provides fundamental insights into the reaction dynamics under isolated conditions free from wall effects and secondary collisions. Hence, this system is particularly intriguing from a physical-organic chemistry perspective, as such compounds help elucidate chemical reactivity, bond dissociation processes, and the cyclization of acyclic precursors into organosilicon rings. This, in turn, opens new avenues for exploring the relatively underdeveloped class of silicon–nitrogen-containing heterocyclic molecules.

Experimental

Crossed molecular beam experiment

The gas-phase reaction between the silicon nitride radical (SiN, $X^2\Sigma^+$) and isoprene (2-methyl-1,3-butadiene; C_5H_8, X^1A') was studied under single-collision conditions exploiting a crossed molecular beam apparatus. The experimental setup, data

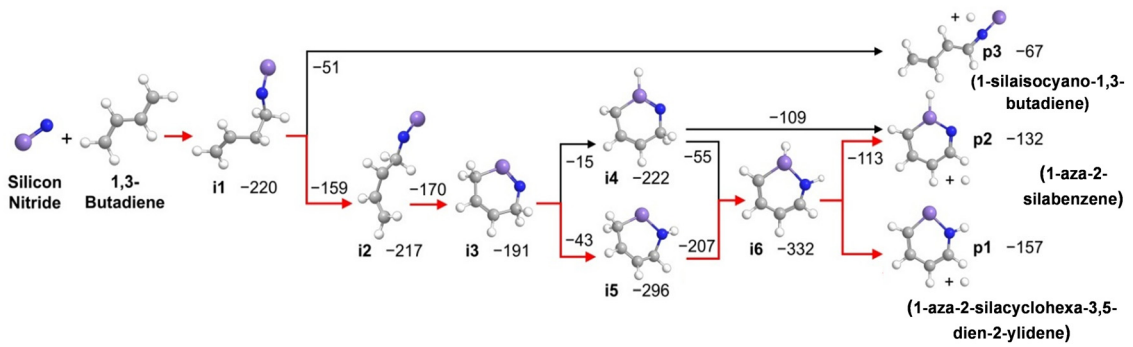

Fig. 1 Mechanistic pathways for the reaction between silicon nitride radical (SiN, $X^2\Sigma^+$) and 1,3-butadiene (C_4H_6, X^1A_g). Red arrows indicate the most probable pathways.[31] Atoms are color-coded as follows: nitrogen (blue), silicon (violet), carbon (grey), and hydrogen (white).

acquisition method, and analysis procedures were described in detail previously.[47–49,52–54] The crossed beams machine consists of a stainless-steel vacuum chamber (10^{-8} Torr) which encloses two source chambers and a triply differentially pumped ultra-high-vacuum (10^{-12} Torr), rotatable, differentially pumped quadrupole mass spectrometric detector (QMS). The pulsed supersonic beam of silicon nitride radicals (SiN, $X^2\Sigma^+$) was generated *in situ* in the primary source by laser ablation (3 mJ, 266 nm, 30 Hz; Quanta-Ray) of a silicon rod (Si, 99.999%, Goodfellow) and subsequent reaction of the ablated species with neat nitrous oxide (N_2O, 99.99%, Matheson) that also acts as seeding gas. The nitrous oxide was released by a Proch–Trickl piezoelectric pulsed valve[55] operated at 60 Hz with a backing pressure of 4 atm. The SiN($X^2\Sigma^+$) radical beam was skimmed and velocity-selected using a four-slot chopper wheel (120 Hz); this achieved a peak velocity v_p = 1204 ± 18 m s^{-1} and speed ratio S = 4.3 ± 0.4. The pulsed secondary molecular beam (60 Hz, v_p = 730 ± 10 m s^{-1}, S = 8.5 ± 0.2) of neat 2-methyl-1,3-butadiene (450 Torr, $CH_2C(CH_3)CHCH_2$; Sigma-Aldrich, 99%) was released 49 μs prior to the primary beam. Both molecular beams intersected at 90° in the scattering chamber at a mean collision energy of E_C = 25 ± 1 kJ mol^{-1}. Note that an attempt was also made to generate silicon nitride radicals (SiN, $X^2\Sigma^+$) by exploiting molecular nitrogen gas. However, this resulted in silicon nitride radical number densities about one order of magnitude lower.[56]

The reactively scattered products were ionized *via* electron ionization at 80 eV (2 mA) at the entrance of the rotatable detector, filtered according to mass-to-charge ratios (m/z) by the QMS (Extrel, QC 150; 2.1 MHz), and detected using a Daly-type particle ion counter.[57] The detector is rotatable in the scattering plane defined by the primary and secondary beams. Angularly resolved time-of-flight (TOF) spectra were recorded at discrete laboratory angles between 29.25° and 59.25°. Operating laser at 30 Hz and the pulsed valve at 60 Hz allowed instant background subtraction (''laser-on'' minus ''laser-off'') during the TOF recording. To gain information on the reaction dynamics, the TOF spectra and the laboratory angular distribution (LAD) were fitted with a forward-convolution technique.[58,59] This approach uses initially a trial angular flux $T(\theta)$ and translational energy $P(E_T)$ distributions in the center-of-mass (CM) frame to simulate the laboratory data (TOFs and LAD). CM functions were then iteratively refined until the best fit of the TOF spectra and LAD was achieved. Together, the CM functions represent the reactive differential cross section $I(\theta, u)$, the CM velocity u, $I(u, \theta) \sim P(u) \times T(\theta)$, which is represented as a flux contour map, thus depicting an overall image of the reaction outcome.

Theoretical calculations

Quantum-chemical calculations were carried out using the Gaussian 16 software package (Revision C.01).[60] Geometries and energies were calculated with the CBS-QB3 composite method by Petersson as included in the Gaussian 16 software package.[61–68] The CBS-QB3 calculations are a five-step procedure, which involves extrapolations to the complete basis set and complete correlation through a series of calculations. In the first step geometries are optimized and frequencies are calculated at the B3LYP/CBSB7 level of theory to obtain thermal corrections, zero-point vibrational energy (ZPVE) corrections, and entropic information.[69–71] In the next steps single point energy calculations are performed at CCSD(T)/6-31 + G(d),[72–76] MP4SDQ/CBSB4[77,78] and MP2/CBSB3[79–83] levels of theory. Final energies are obtained after extrapolation to the complete basis set. The overall charge and multiplicity were 0 and 2 for the SiN and isoprene system, respectively. All stationary points on the potential energy surface (PES) were characterized by harmonic vibrational frequency analysis. All minima were confirmed by the absence of imaginary frequencies, while all transition states exhibited exactly one imaginary frequency corresponding to motion along the reaction coordinate. For each TS, intrinsic reaction coordinate (IRC) calculations verified connectivity to the intended reactant and product minima. The energies depicted in Fig. 4 and 5 are reported as $E_0 = E_{electronic}$ + ZPVE. We used CBS-QB3 because it delivers near-CCSD(T)/CBS thermochemistry at roughly chemical-accuracy for small main-group systems while remaining practical for mapping full PESs. This is ideal for deriving reliable 0 K thresholds and barrier heights for the SiN + isoprene surface without the cost of full CCSD(T)/CBS optimizations.

Results and discussion

Laboratory angular distribution

Reactive scattering signal of the bimolecular gas-phase reaction of the silicon nitride radical (SiN, $X^2\Sigma^+$; 42 amu) with isoprene ($CH_2C(CH_3)CHCH_2$; X^1A'; 68 amu) was monitored at m/z = 109 ($SiNC_5H_7^+$), 108 ($SiNC_5H_6^+$), and 95 ($SiNC_4H_5^+$) for potential atomic hydrogen, molecular hydrogen, and methyl elimination channels, respectively. Signal was only detected at m/z = 109, suggesting the presence of only the atomic hydrogen loss reaction channel (reaction (1)).

$$SiN(42\ amu) + C_5H_8(68\ amu) \rightarrow SiNC_5H_7(109\ amu) + H(1\ amu) \quad (1)$$

The corresponding laboratory angular distribution (LAD) was extracted by integrating TOF spectra recorded at m/z = 109 at distinct laboratory angles from 29.25° to 59.25° in intervals of 5°. Notable features of the LAD (Fig. 2a) include its width of at least 30° and symmetry around the CM angle at 44.3 ± 0.5°. These findings propose that the $SiNC_5H_7$ products were formed *via* indirect scattering dynamics through complex formation involving one or more $SiNC_5H_8$ intermediates. The ion signal in the TOF spectra was spread over approximately 250 μs, ranging from 650 μs to 900 μs (Fig. 2b). Overall, the laboratory data suggest the exclusive gas-phase preparation of $SiNC_5H_7$ isomer(s) *via* the elementary gas-phase reaction of the silicon nitride radical (SiN, $C_{\infty v}$, $X^2\Sigma^+$) with isoprene (C_5H_8, C_{2h}, X^1A').

Center of mass frame

To gain information on the reaction mechanisms, a forward-convolution routine is exploited to convert the laboratory data

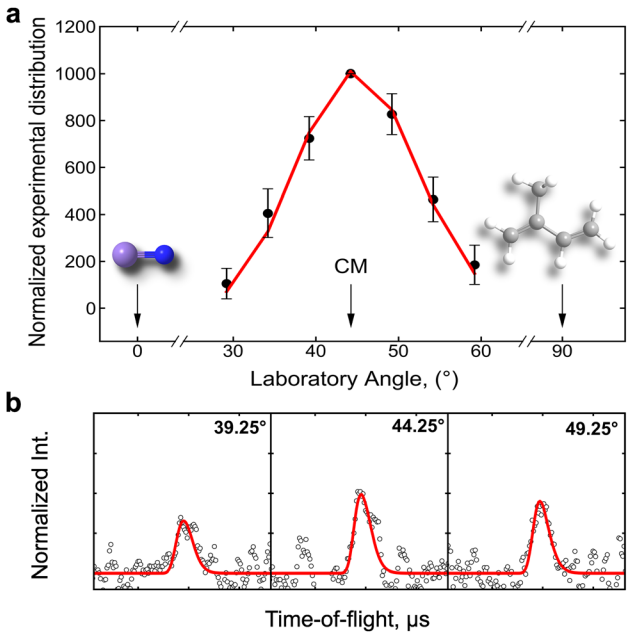

Fig. 2 (a) Laboratory angular distribution and (b) time-of-flight (TOF) spectra recorded at m/z = 109 for the reaction between silicon nitride (SiN, $X^2\Sigma^+$) and isoprene (2-methyl-1,3-butadiene, C_5H_8, X^1A'). In (a), the solid circles with error bars represent the normalized experimental distribution with $\pm 1\sigma$ uncertainty (standard deviation of the TOF integrals for each angle), while in b), the experimental data are shown as open black circles. For each angle, 1×10^6 TOF spectra (10 h total acquisition) were averaged to achieve an adequate signal-to-noise ratio. The red solid lines in (a) and (b) correspond to the best-fit results from the forward-convolution routine. Atoms are color-coded in blue (nitrogen), violet (silicon), grey (carbon), and white(hydrogen).

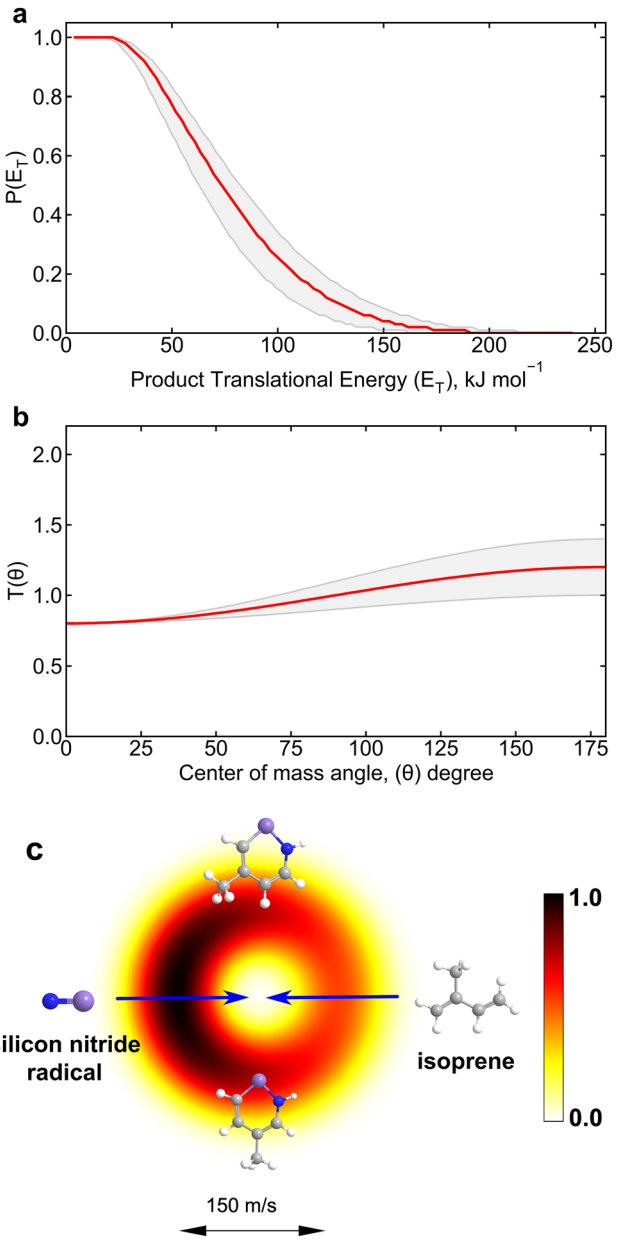

Fig. 3 (a) Center-of-mass translational energy distribution $P(E_T)$, (b) the angular flux distribution $T(\theta)$, and (c) the flux contour map (top view) leading to the formation of silicon nitrogen containing heterocyclic products from the reaction between ground state silicon nitride silicon nitride (SiN, $X^2\Sigma^+$) and isoprene (C_5H_8, X^1A'). Solid red lines represent the best-fit results, while shaded regions indicate the associated uncertainties. The direction of the silicon nitride beam is defined as 0°, and that of isoprene as 180°. Atoms are color-coded as follows: nitrogen (blue), silicon (violet), carbon (grey), and hydrogen (white).

(TOFs, LADs) into the center-of-mass (CM) reference frame.[58,59] The laboratory data could be fit with a single channel (reaction (1)) with an energy-dependent reaction cross section proportional to $E_C^{-(2/3)}$ for entrance-barrierless reactions dominated by long-range dipole–dipole interactions.[84] The best-fit CM functions are depicted in Fig. 3, where the grey-filled areas define the limits of the acceptable fits. Considering the translational energy flux distribution $P(E_T)$ (Fig. 3a), the maximum energy (E_{max}) represents the kinetic energy of those molecules born without internal excitation. The energy conservation dictates that $E_{max} = E_C - \Delta_r G$, where E_C and $\Delta_r G$ represent the collision energy and the reaction energy, respectively. The derived $P(E_T)$ terminates at 187 ± 26 kJ mol^{-1}. Subtracting this E_{max} from the experimental collision energy of 25 ± 1 kJ mol^{-1} yields an exoergicity of $\Delta_r G$ = −162 ± 27 kJ mol^{-1} for the atomic hydrogen loss channel. In addition, the distribution maximum of the $P(E_T)$ shows a plateau from 0 to some 25 kJ mol^{-1}, indicating the likely existence of both loose and tight exit transition states.[84] The average translation energy of 48.6 ± 6.3 kJ mol^{-1} suggests further that 26.1 ± 7.0% of the total energy is channeled into product translation, which implies the formation of a covalently bound, long-lived intermediate.[84] The $T(\theta)$ distribution contains additional information on the underlying reaction dynamics. The CM angular flux distribution (Fig. 3b) shows intensity over the full angular range, additionally supporting the indirect scattering dynamics *via* complex formation. The $T(\theta)$ also displays a slight backward scattering with respect to the radical beam, with an intensity ratio $I(0°)/I(180°)$ of (0.7 ± 0.1) : 1. This suggests that at least one reaction channel proceeds *via* a rebound mechanism[85] and/or a short-lived $SiNC_5H_8$ reaction intermediate ejecting the atomic hydrogen. These findings are also depicted in the flux velocity–angle contour map (Fig. 3c), which provides an overall image of the reactive scattering processes.

Electronic structure calculation

In case of complex, polyatomic systems, it is beneficial to combine the experimental data with a computational investigation of the underlying potential energy surface (PES). In total, 38 product isomers **P1–P38** were examined to identify the most probable reaction channel (Fig. 4). Among the products explored, **P1–P4** are six-membered cyclic structures, **P5–P8** carry a five-membered ring, and the remaining isomers are acyclic. The calculated reaction energies are in the range from −157 to +200 kJ mol^{-1}. The experimental reaction energy (−162 ± 27 kJ mol^{-1}) with respect to separated reactants correlates well with two thermodynamically most stable product isomers, **P1** (4-methyl-1-aza-2-silacyclohexa-3,5-dien-2-ylidene; −156 kJ mol^{-1}, Cs, X^1A') and **P2** (5-methyl-1-aza-2-silacyclohexa-3,5-dien-2-ylidene; −150 kJ mol^{-1}, Cs, X^1A'); both carry six-membered rings with adjacent silicon and nitrogen atoms. Based on the energetics, both isomers are likely products of the reaction between silicon nitride radical (SiN) and isoprene (C_5H_8), in line with previous observations from the reaction of silicon nitride radical (SiN) with 1,3-butadiene (C_4H_6).[36] That reaction was initiated by a barrierless addition of the silicon nitride radical *via* its nitrogen center, followed by isomerization and cyclization to form a cyclic C_4H_6NSi intermediate, ultimately eliminating a hydrogen atom to yield six-membered heterocyclic azasilabenzenes (Fig. 1). Addition through the silicon center at the initial step was found to involve a substantial entrance barrier of 31 kJ mol^{-1}, which was not accessible with experimental collision energy (24.0 ± 0.5 kJ mol^{-1}). Given the structural similarity between 1,3-butadiene (C_4H_6) and isoprene (C_5H_8) – methyl-substituted 1,3-butadiene derivative – comparable mechanistic

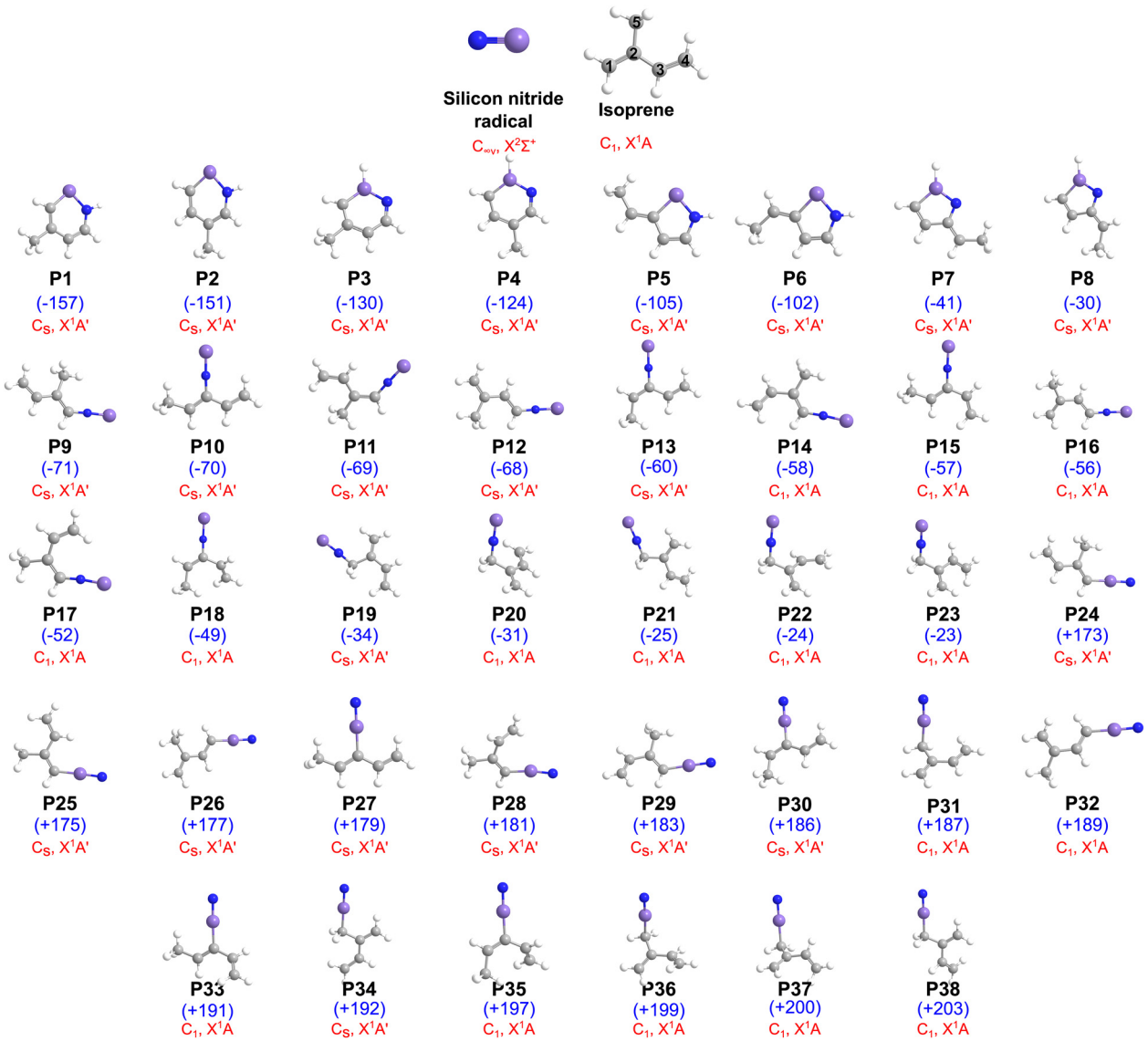

Fig. 4 Optimized geometries of the reactants and the possible product isomers from the reaction of silicon nitride radical (SiN, $X^2\Sigma^+$) with isoprene (C_5H_8, X^1A'), computed with CBS-QB3 composite method. Relative energies (in kJ mol^{-1}) with respect to the separated reactants are provided in parentheses (blue colors). Texts in red color represent the symmetry and the electronic states of the isomers. Atom colors are designated as follows: nitrogen (blue), silicon (violet), carbon (gray), and hydrogen (white).

pathways are expected. The experimental collision energy of the reaction of silicon nitride radical (SiN, $X^2\Sigma^+$) and isoprene (C_5H_8, X^1A') is similar to the collision energy for the reaction of silicon nitride radical (SiN, $X^2\Sigma^+$) and 1,3 butadiene (C_4H_6, X^1A_g).[36] In contrast to 1,3-butadiene, isoprene possesses a methyl substituent, which breaks the symmetry of the π-system and leads to multiple nonequivalent reactive centers. As a result, the SiN plus isoprene reaction exhibits a larger number of entrance channels, intermediates, and product isomers compared to the SiN plus 1,3-butadiene system. Overall, mechanism of reaction of SiN and isoprene most likely forms an acyclic addition intermediate through carbon–nitrogen bond formation, where the nitrogen atom of the radical attacks one of the terminal carbon atoms of isoprene; note the sterical effect of the methyl group, which facilitates a doublet radical addition to the sterically more accessible C1 and C4 positions of the 1,3-butadiene moiety.[22,86–93] These intermediates subsequently undergo cyclization and isomerization *via* hydrogen migration followed by atomic hydrogen elimination to **P1** and **P2**.

Fig. 5 presents the potential energy surfaces (Paths **I** and **II**) for the formation of the two most probable products: 4-methyl-1-aza-2-silacyclohexa-3,5-dien-2-ylidene (**P1**) and 5-methyl-1-aza-2-silacyclohexa-3,5-dien-2-ylidene (**P2**). Considering Path **I**, the reaction is initiated with the barrierless addition of the silicon nitride radical (SiN) with the nitrogen atom to the terminal carbon atom of isoprene, yielding the acyclic **i1-*trans*** (C_1, X^2A) intermediate. The **i1-*trans*** intermediate subsequently isomerizes to **i1-*cis*** (C_1, X^2A) followed by ring closure to a six-membered ring, generating **i2** (C_s, X^2A'). Intermediate **i2** can then evolve either to **i3** (C_s, X^2A'') *via* a hydrogen shift from the C1 carbon of the 1,3-butadiene moiety to the silicon atom

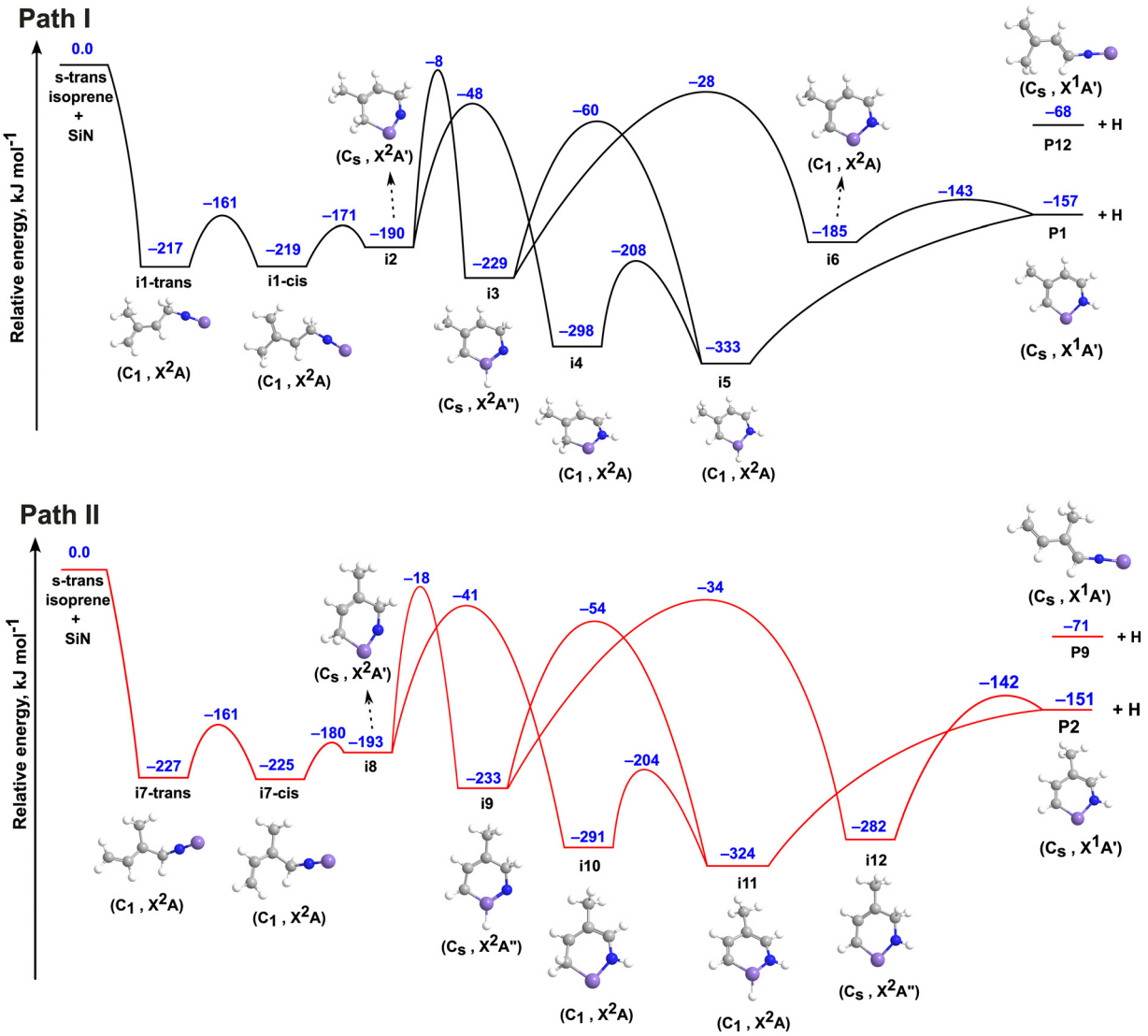

Fig. 5 Potential energy surface of the reaction silicon nitride radical (SiN, $C_{\infty v}$, $X^2\Sigma^+$) and isoprene (C_5H_8, X^1A') where solid black and red lines represent the doublet surface. Path **I** and **II** are two mechanistic pathways depending on the initialization step involving the addition of the silicon nitride radical (SiN) to either of the terminal carbon atoms in isoprene (C_5H_8). The numbers in blue color denote energies (in kJ mol^{-1}) for each species calculated with CBS-QB3 composite method. Atoms are color-coded in purple (silicon), blue (nitrogen), grey (carbon), and white (hydrogen).

overcoming a barrier of 182 kJ mol^{-1}, or to **i4** (C_1, X^2A) through a hydrogen shift to the nitrogen atom with the transition state lying 140 kJ mol^{-1} above the **i2**. From **i3**, two distinct pathways are accessible: a hydrogen migration from the C4 carbon atom to nitrogen, leading to **i5** (C_1, X^2A) or a hydrogen shift from silicon to nitrogen, forming **i6** (C_1, X^2A). Intermediate **i5** may also arise from **i4** *via* a hydrogen shift from the C1 carbon atom to silicon. Unimolecular decomposition of **i5** yields **P1** (C_s, X^1A') *via* atomic hydrogen elimination from silicon along with a barrierless exit channel. On the other hand, **i6** undergoes unimolecular decomposition to form **P1** *via* atomic hydrogen loss by overcoming a transition state 14 kJ mol^{-1} above the dissociated products. Overall, the methyl group is not involved in the reaction pathway to **P1** and hence acts as a spectator.

With respect to Path **II**, the reaction once again commences with a barrierless addition of the SiN radical with its nitrogen center but to the C1 carbon atom of isoprene, forming the **i7-*trans*** (C_1, X^2A) collision complex. **i7-*trans*** then isomerizes to **i7-*cis*** (C_1, X^2A) and undergoes ring-closure to **i8** (C_s, X^2A'). From **i8**, two hydrogen shift paths are accessible: one from the C4 carbon atom to the silicon atom to **i9** (C_s, X^2A''), and a second option from the C1 carbon atom of the 1.3-butadiene moiety to the nitrogen atom, yielding **i10** (C_1, X^2A). Intermediate **i9** may further isomerize to **i11** (C_1, X^2A) *via* a hydrogen shift from the C1 carbon atom to nitrogen, or it may convert to **i12** (C_s, X^2A'') through a hydrogen migration from silicon to nitrogen. On the other hand, **i10** undergoes a hydrogen shift from the C4 carbon atom to the silicon atom, forming the **i11** intermediate. Finally, **i11** leads to product **P2** (C_s, X^1A') through a barrierless atomic hydrogen elimination channel. The same product, **P2**, can also be formed from **i12** *via* atomic hydrogen elimination, with a tighter exit transition state 9 kJ mol^{-1} above the products.

Both Path **I** and Path **II** proceed through a tight exit barrier as well as a barrierless exit channel, which aligns well with the plateau observed in the experimentally derived translational energy flux distribution (Fig. 3a). Since all the transition states lie well below the limit of our collision energy, all the pathways are energetically accessible for product formation. However, in Path **I**, the transition energy for **i2** → **i3** (182 kJ mol^{-1}) is higher than that for **i2** → **i4** (140 kJ mol^{-1}), indicating that the latter step is energetically more favorable. In Path **II**, the **i8** → **i9** isomerization, which involved a barrier of 175 mol^{-1}, is less favorable than the **i8** → **i10** step, which has a lower barrier of only 152 mol^{-1}. Overall, for Path **I**, the sequence **i1-*trans*** → **i1-*cis*** → **i2** → **i4** → **i5** → **P1** + H, and for Path **II**, the reaction path **i7-*trans*** → **i7-*cis*** → **i8** → **i10** → **i11** → **P2** + H represent the more favorable reaction routes (Fig. 5). Once again, the methyl group is not involved in the reaction dynamics to **P2** and hence acts as a spectator. Note that the overall reactions to the acyclic products (*E*)-1-silaisocyano-3-methylbuta-1,3-dien (**P12**, C_s, X^1A') and (*E*)-1-silaisocyano-2-methylbuta-1,3-dien (**P9**, C_s, X^1A') originating from the hydrogen loss of the initial collision complexes **i1-*trans*** and **i7-*trans*** are exoergic by 68 kJ mol^{-1} and 71 kJ mol^{-1} (Fig. 4); these products could be hidden in the low energy tail of the center-of-mass translational energy distribution.

In exploring the potential energy surface (PES), SiN addition to all symmetry-inequivalent carbon atoms of isoprene was considered. However, reaction pathways were retained only when the associated reaction energies were accessible within the experimental collision energy ($\leq E_{(c)} \approx 24.0 \pm 0.5$ kJ mol^{-1}). Notably, ring-closure pathways leading to six-membered heterocycles were identified exclusively for intermediates formed *via* terminal carbon addition. No energetically viable cyclization pathways were found for non-terminal addition channels within the accessible energy window. The primary objective of this work is to elucidate the reaction dynamics of cyclization channels leading to silicon–nitrogen-containing heterocycles. Accordingly, a complete mapping of the PES for all possible products was not pursued, particularly for acyclic product-formation pathways, which are computationally demanding and beyond the scope of understanding the dynamics of heterocycle formation. We note that additional reaction channels may exist in principle; however, based on the energetic thresholds imposed by the collision energy and barrier heights, these channels are not expected to contribute measurably under single-collision crossed molecular beam conditions.

Conclusions

The elementary reaction between the ground state silicon nitride radical (SiN, $X^2\Sigma^+$) and isoprene (C_5H_8, X^1A') was investigated exploiting a crossed molecular beam apparatus under single collision conditions at a collision energy of 25 ± 1 kJ mol^{-1}. At this collision energy, the comparison of the experimental and computational reaction energies indicates that the reaction proceeds at least *via* two hydrogen-loss channels leading to the formation of two cyclic isomers belonging to the previously elusive class of methylazasilacyclohexadienylidenes: 4-methyl-1-aza-2-silacyclohexa-3,5-dien-2-ylidene (**P1**) and 5-methyl-1-aza-2-silacyclohexa-3,5-dien-2-ylidene (**P2**). Both reaction channels proceed barrierlessly through the addition of the silicon nitride radical with its nitrogen radical *via* indirect reaction mechanisms involving long-lived intermediates ($SiNC_5H_8$). The data also indicate the presence of both barrierless and barrier-mediated exit channels, as evidenced by the plateau observed in the center-of-mass translational energy flux distribution. Consistent with the reaction of the silicon nitride (SiN) radical with 1,3-butadiene (C_4H_6), the present reaction proceeds through a barrierless addition of the SiN radical to either terminal carbon atom of trans-isoprene *via* the nitrogen center, followed by isomerization to the *cis* isomer, cyclization, and successive hydrogen-shifts ultimately leading *via* unimolecular decomposition through hydrogen elimination to the six membered ringed products. However, in comparison with the reaction between silicon nitride and 1,3-butadiene, important differences arise due to the asymmetric substitution in isoprene. These silicon-containing heterocycles are of considerable interest due to their potential applications in medicinal and agrochemical research, thus providing new mechanistic insights into the formation of a unique class of silicon-containing heterocyclic molecules, thereby broadening the scope of organosilicon chemistry.

Author contributions

Supervision and funding acquisition – R. I. K. and A. K. E.; formal analysis – S. M.; investigation – S. M., I. A. M., D. G., and S. J. G. carried out the experimental measurements; A. K. E. – carried out the theoretical analysis; writing original draft – S. M.; writing – review & editing – S. M., R. I. K., A. K. E.

Conflicts of interest

There are no conflicts to declare.

Data availability

The data supporting the findings of this study are available within the article and the supplementary information (SI). Supplementary information: the supplementary material contains details of the optimized Cartesian coordinates (Å) for all isomers of the reaction product, reactants, and intermediates involved in the SiN + C_5H_8 reaction.

Acknowledgements

The experimental work at the University of Hawai'i at Manoa was supported by the National Science Foundation (NSF) CHE 2244717. The quantum chemical calculations in Bochum were supported by the Deutsche Forschungsgemeinschaft (DFG, German Research Foundation) under Germany's Excellence Strategy – EXC 2033 – 390677874 – RESOLV.

References

1 C. Thebtaranonth and Y. Thebtaranonth, *Cyclization reactions*, CRC Press, 1993.
2 J. A. Joule, *Heterocyclic chemistry*, CRC Press, 2020.
3 E. G. Brown, *Ring nitrogen and key biomolecules: The biochemistry of N-heterocycles*, Springer Science & Business Media, 1998.
4 B. Giese, B. Kopping, T. Göbel, J. Dickhaut, G. Thoma, K. J. Kulicke and F. Trach, *Org. React.*, 2004, **48**, 301–856.
5 R. I. Kaiser, D. S. Parker and A. M. Mebel, *Annu. Rev. Phys. Chem.*, 2015, **66**, 43–67.
6 R. I. Kaiser and A. M. Mebel, *Chem. Soc. Rev.*, 2012, **41**, 5490–5501.
7 R. Kaiser, I. Hahndorf, L. Huang, Y. Lee, H. Bettinger, P. V. R. Schleyer, H. Schaefer III and P. Schreiner, *J. Chem. Phys.*, 1999, **110**, 6091–6094.
8 R. Kaiser, A. Mebel and Y. Lee, *J. Chem. Phys.*, 2001, **114**, 231–239.
9 J. Lang, C. D. Foley, S. Thawoos, A. Behzadfar, Y. Liu, J. Zádor and A. G. Suits, *Faraday Discuss.*, 2024, **251**, 550–572.
10 H. Li, J. Lang, C. D. Foley, J. Zádor and A. G. Suits, *J. Phys. Chem. Lett.*, 2023, **14**, 7611–7617.
11 T. Yang, B. B. Dangi, A. M. Thomas, B. J. Sun, T. J. Chou, A. H. Chang and R. I. Kaiser, *Angew. Chem.*, 2016, **128**, 8115–8119.
12 S. J. Barraza and S. E. Denmark, *J. Am. Chem. Soc.*, 2018, **140**, 6668–6684.
13 N. J. Hill and R. West, *J. Organomet. Chem.*, 2004, **689**, 4165–4183.
14 M. Denk, R. Lennon, R. Hayashi, R. West, A. V. Belyakov, H. P. Verne, A. Haaland, M. Wagner and N. Metzler, *J. Am. Chem. Soc.*, 1994, **116**, 2691–2692.
15 Y. Chen, J. Li, Y. Zhao, L. Zhang, G. Tan, H. Zhu and H. W. Roesky, *J. Am. Chem. Soc.*, 2021, **143**, 2212–2216.
16 M. Kira, S. Ishida, T. Iwamoto and C. Kabuto, *J. Am. Chem. Soc.*, 1999, **121**, 9722–9723.
17 K. Wakita, N. Tokitoh, R. Okazaki, S. Nagase, P. V. R. Schleyer and H. Jiao, *J. Am. Chem. Soc.*, 1999, **121**, 11336–11344.
18 T. J. Barton and G. T. Burns, *J. Am. Chem. Soc.*, 1978, **100**, 5246.
19 T. M. Gentle and E. L. Muetterties, *J. Am. Chem. Soc.*, 1983, **105**, 304–305.
20 K. Wakita, N. Tokitoh, R. Okazaki, N. Takagi and S. Nagase, *J. Am. Chem. Soc.*, 2000, **122**, 5648–5649.
21 G. R. Jachak, R. Ramesh, D. G. Sant, S. U. Jorwekar, M. R. Jadhav, S. G. Tupe, M. V. Deshpande and D. S. Reddy, *ACS Med. Chem. Lett.*, 2015, **6**, 1111–1116.
22 Z. Yang, C. He, S. Goettl and R. I. Kaiser, *J. Phys. Chem. A*, 2021, **125**, 5040–5047.
23 R. A. Benkeser, Y. Nagai, J. L. Noe, R. F. Cunico and P. H. Gund, *J. Am. Chem. Soc.*, 1964, **86**, 2446–2451.
24 M. Bols and T. Skrydstrup, *Chem. Rev.*, 1995, **95**, 1253–1277.
25 D. Wittenberg and H. Gilman, *J. Am. Chem. Soc.*, 1958, **80**, 2677–2680.
26 I. Langmuir, *J. Am. Chem. Soc.*, 1919, **41**, 868–934.
27 J. Clayden, N. Greeves and S. Warren, *Organic chemistry*, Oxford university press, 2012.
28 A. K. Franz and S. O. Wilson, *J. Med. Chem.*, 2013, **56**, 388–405.
29 J. Y. Corey, *Chem. Org. Silicon Compd.*, 1989, **1**, 1–56.
30 S. Deerenberg, M. Schakel, A. H. de Keijzer, M. Kranenburg, M. Lutz, A. L. Spek and K. Lammertsma, *Chem. Commun.*, 2002, 348–349.
31 B. Marciniec and J. Chojnowski, *Progress in organosilicon chemistry*, Taylor & Francis, 1995.
32 F. Kleemiss, P. Puylaert, D. Duvinage, M. Fugel, K. Sugimoto, J. Beckmann and S. Grabowsky, *Struct. Sci.*, 2021, **77**, 892–905.
33 S. M. Sieburth, *Designing Safer Chemicals*, American Chemical Society, 1996, vol. 640, ch. 4, pp. 74–83.
34 R. Ramesh and D. S. Reddy, *J. Med. Chem.*, 2017, **61**, 3779–3798.
35 R. Tacke, F. Popp, B. Müller, B. Theis, C. Burschka, A. Hamacher, M. U. Kassack, D. Schepmann, B. Wünsch and U. Jurva, *ChemMedChem*, 2008, **3**, 152–164.
36 S. Metya, I. A. Medvedkov, S. J. Goettl, T. Sattasathuchana, M. X. Silva, B. R. L. Galvão and R. I. Kaiser, *Angew. Chem., Int. Ed.*, 2025, e17656.
37 S. B. Morales, C. J. Bennett, S. D. Le Picard, A. Canosa, I. R. Sims, B. Sun, P. Chen, A. H. Chang, V. V. Kislov and A. M. Mebel, *Astrophys. J.*, 2011, **742**, 26.

38 B. Sun, C. Huang, S. Chen, S. Chen, R. Kaiser and A. Chang, *J. Phys. Chem. A*, 2014, **118**, 7715–7724.
39 L. Huang, O. Asvany, A. Chang, N. Balucani, S. Lin, Y. Lee, R. I. Kaiser and Y. Osamura, *J. Chem. Phys.*, 2000, **113**, 8656–8666.
40 N. Balucani, O. Asvany, A. Chang, S. Lin, Y. Lee, R. Kaiser and Y. Osamura, *J. Chem. Phys.*, 2000, **113**, 8643–8655.
41 L. C. L. Huang, N. Balucani, Y. T. Lee, R. I. Kaiser and Y. Osamura, *J. Chem. Phys.*, 1999, **111**, 2857–2860.
42 N. Balucani, O. Asvany, A. Chang, S. Lin, Y. Lee, R. Kaiser, H. Bettinger, P. V. R. Schleyer and H. Schaefer III, *J. Chem. Phys.*, 1999, **111**, 7457–7471.
43 D. Parker, A. Wilson, R. Kaiser, T. Labrador and A. Mebel, *J. Org. Chem.*, 2012, **77**, 8574–8580.
44 D. S. Parker, A. V. Wilson, R. I. Kaiser, T. Labrador and A. M. Mebel, *J. Am. Chem. Soc.*, 2012, **134**, 13896–13901.
45 R. I. Kaiser, D. Stranges, H. M. Bevsek, Y. T. Lee and A. G. Suits, *J. Chem. Phys.*, 1997, **106**, 4945–4953.
46 X. Gu and R. I. Kaiser, *Acc. Chem. Res.*, 2009, **42**, 290–302.
47 R. I. Kaiser, *Chem. Rev.*, 2002, **102**, 1309–1358.
48 R. I. Kaiser, A. M. Mebel, A. H. H. Chang, S. H. Lin and Y. T. Lee, *J. Chem. Phys.*, 1999, **110**, 10330–10344.
49 R. I. Kaiser, I. Hahndorf, L. C. L. Huang, Y. T. Lee, H. F. Bettinger, P. V. R. Schleyer, H. F. SchaeferIII and P. R. Schreiner, *J. Chem. Phys.*, 1999, **110**, 6091–6094.
50 Y. T. Lee, *Angew. Chem., Int. Ed. Engl.*, 1987, **26**, 939–951.
51 D. R. Herschbach, *Angew. Chem., Int. Ed. Engl.*, 1987, **26**, 1221–1243.
52 R. Kaiser and X. Gu, *J. Chem. Phys.*, 2009, **131**, 104311.
53 S. J. Goettl, S. Doddipatla, Z. Yang, C. He, R. I. Kaiser, M. X. Silva, B. R. Galvao and T. J. Millar, *Phys. Chem. Chem. Phys.*, 2021, **23**, 13647–13661.
54 R. I. Kaiser, P. Maksyutenko, C. Ennis, F. Zhang, X. Gu, S. P. Krishtal, A. M. Mebel, O. Kostko and M. Ahmed, *Faraday Discuss.*, 2010, **147**, 429–478.
55 D. Proch and T. Trickl, *Rev. Sci. Instrum.*, 1989, **60**, 713–716.
56 D. Parker, A. Mebel and R. Kaiser, *Chem. Soc. Rev.*, 2014, **43**, 2701–2713.
57 N. Daly, *Rev. Sci. Instrum.*, 1960, **31**, 264–267.
58 M. F. Vernon, *Molecular beam scattering*, University of California, Berkeley, 1983.
59 P. S. Weiss, PhD Dissertation, University of California, Berkeley, CA, 1986.
60 M. J. Frisch, G. W. Trucks, H. B. Schlegel, G. E. Scuseria, M. A. Robb, J. R. Cheeseman, G. Scalmani, V. Barone, G. A. Petersson, H. Nakatsuji, X. Li, M. Caricato, A. V. Marenich, J. Bloino, B. G. Janesko, R. Gomperts, B. Mennucci, H. P. Hratchian, J. V. Ortiz, A. F. Izmaylov, J. L. Sonnenberg Williams, F. Ding, F. Lipparini, F. Egidi, J. Goings, B. Peng, A. Petrone, T. Henderson, D. Ranasinghe, V. G. Zakrzewski, J. Gao, N. Rega, G. Zheng, W. Liang, M. Hada, M. Ehara, K. Toyota, R. Fukuda, J. Hasegawa, M. Ishida, T. Nakajima, Y. Honda, O. Kitao, H. Nakai, T. Vreven, K. Throssell, J. A. Montgomery Jr., J. E. Peralta, F. Ogliaro, M. J. Bearpark, J. J. Heyd, E. N. Brothers, K. N. Kudin, V. N. Staroverov, T. A. Keith, R. Kobayashi, J. Normand, K. Raghavachari, A. P. Rendell, J. C. Burant, S. S. Iyengar, J. Tomasi, M. Cossi, J. M. Millam, M. Klene, C. Adamo, R. Cammi, J. W. Ochterski, R. L. Martin, K. Morokuma, O. Farkas, J. B. Foresman and D. J. Fox, *Gaussian 16 Revision C.01*, Gaussian Inc., Wallingford, CT, 2016.
61 A. Petersson, A. Bennett, T. G. Tensfeldt, M. A. Al-Laham, W. A. Shirley and J. Mantzaris, *J. Chem. Phys.*, 1988, **89**, 2193–2218.
62 G. A. Petersson and M. A. Al-Laham, *J. Chem. Phys.*, 1991, **94**, 6081–6090.
63 G. A. Petersson, T. G. Tensfeldt and J. A. Montgomery Jr, *J. Chem. Phys.*, 1991, **94**, 6091–6101.
64 J. A. Montgomery Jr, J. W. Ochterski and G. A. Petersson, *J. Chem. Phys.*, 1994, **101**, 5900–5909.
65 J. W. Ochterski, G. A. Petersson and K. B. Wiberg, *J. Am. Chem. Soc.*, 1995, **117**, 11299–11308.
66 J. W. Ochterski, G. A. Petersson and J. A. Montgomery Jr, *J. Chem. Phys.*, 1996, **104**, 2598–2619.
67 J. A. Montgomery Jr, M. J. Frisch, J. W. Ochterski and G. A. Petersson, *J. Chem. Phys.*, 1999, **110**, 2822–2827.
68 J. A. Montgomery Jr, M. J. Frisch, J. W. Ochterski and G. A. Petersson, *J. Chem. Phys.*, 2000, **112**, 6532–6542.
69 A. D. Becke, *Phys. Rev. A:At., Mol., Opt. Phys.*, 1988, **38**, 3098.
70 C. Lee, W. Yang and R. G. Parr, *Phys. Rev. B:Condens. Matter Mater. Phys.*, 1988, **37**, 785.
71 A. D. Becke, *J. Chem. Phys.*, 1993, **98**, 5648–5652.
72 J. Čížek, *J. Chem. Phys.*, 1966, **45**, 4256–4266.
73 M. Urban, J. Noga, S. J. Cole and R. J. Bartlett, *J. Chem. Phys.*, 1985, **83**, 4041–4046.
74 K. Raghavachari, G. W. Trucks, J. A. Pople and M. Head-Gordon, *Chem. Phys. Lett.*, 1989, **157**, 479–483.
75 R. J. Bartlett, J. Watts, S. Kucharski and J. Noga, *Chem. Phys. Lett.*, 1990, **165**, 513–522.
76 J. F. Stanton, *Chem. Phys. Lett.*, 1997, **281**, 130–134.
77 R. Krishnan and J. A. Pople, *Int. J. Quantum Chem.*, 1978, **14**, 91–100.
78 R. Krishnan, M. J. Frisch and J. A. Pople, *J. Chem. Phys.*, 1980, **72**, 4244–4245.
79 M. Head-Gordon, J. A. Pople and M. J. Frisch, *Chem. Phys. Lett.*, 1988, **153**, 503–506.
80 S. Sæbø and J. Almlöf, *Chem. Phys. Lett.*, 1989, **154**, 83–89.
81 M. J. Frisch, M. Head-Gordon and J. A. Pople, *Chem. Phys. Lett.*, 1990, **166**, 275–280.
82 M. J. Frisch, M. Head-Gordon and J. A. Pople, *Chem. Phys. Lett.*, 1990, **166**, 281–289.
83 M. Head-Gordon and T. Head-Gordon, *Chem. Phys. Lett.*, 1994, **220**, 122–128.
84 R. D. Levine and R. B. Bernstein, *Molecular Reaction Dynamics and Chemical Reactivity*, Oxford University Press, Oxford, 1987.
85 W. Miller, S. Safron and D. Herschbach, *Discuss. Faraday Soc.*, 1967, **44**, 108–122.
86 S. J. Goettl, C. He, Z. Yang, R. I. Kaiser, A. Somani, A. Portela-Gonzalez, W. Sander, B.-J. Sun, S. Fatimah and K. P. Kadam, *Phys. Chem. Chem. Phys.*, 2024, **26**, 18321–18332.
87 B. B. Dangi, T. Yang, R. I. Kaiser and A. M. Mebel, *Phys. Chem. Chem. Phys.*, 2014, **16**, 16805–16814.

88 T. Yang, L. Muzangwa, D. S. Parker, R. I. Kaiser and A. M. Mebel, *Phys. Chem. Chem. Phys.*, 2015, **17**, 530–540.
89 I. A. Medvedkov, Z. Yang, A. A. Nikolayev, S. J. Goettl, A. K. Eckhardt, A. M. Mebel and R. I. Kaiser, *J. Phys. Chem. Lett.*, 2025, **16**, 658–666.
90 B. B. Dangi, D. S. Parker, R. I. Kaiser, A. Jamal and A. M. Mebel, *Angew. Chem., Int. Ed.*, 2013, **52**, 7186–7189.
91 I. A. Medvedkov, Z. Yang, S. J. Goettl and R. I. Kaiser, *J. Phys. Chem. A*, 2025, **129**, 3280–3288.
92 B. B. Dangi, D. S. Parker, T. Yang, R. I. Kaiser and A. M. Mebel, *Angew. Chem.*, 2014, **126**, 4696–4701.
93 I. A. Medvedkov, A. A. Nikolayev, C. He, Z. Yang, A. M. Mebel and R. I. Kaiser, *Angew. Chem.*, 2024, **136**, e202315147.